ACADEMIC PRESS

Journal of Solid State Chemistry 169 (2002) 66–74

JOURNAL OF SOLID STATE CHEMISTRY

www.academicpress.com

Synthesis of orthorhombic $LiMnO_2$ by solid-phase reaction under steam atmosphere and a study of its heat and acid-treated phases

Ramesh Chitrakar,* Kohji Sakane, Aya Umeno, Shuji Kasaishi, Norio Takagi, and Kenta Ooi[1]

Institute for Marine Resources and Environment, National Institute of Advanced Industrial Science & Technology, AIST-Shikoku, 2217-14 Hayashi-cho, Takamatsu 761-0395, Japan

Received 19 March 2002; received in revised form 5 June 2002; accepted 20 August 2002

Abstract

Low crystalline orthorhombic $LiMnO_2$ (*o*-$LiMnO_2$) samples were synthesized by reacting either γ-MnOOH or Mn_2O_3 with $LiOH \cdot H_2O$ in the solid phase under steam atmosphere at 120°C. In the closed system, the vapor arising from $LiOH \cdot H_2O$ may strengthen the reactivity of LiOH at the surface of MnOOH or Mn_2O_3 particles, which may enable slow diffusion of Li^+ ions forming $LiMnO_2$. These samples were compared with crystalline *o*-$LiMnO_2$ prepared by a solid-state reaction method at 700°C in nitrogen gas. The powder X-ray diffraction patterns of low crystalline samples after heating at 400°C in air revealed the formation of a single phase of cubic $Li_{1.6}Mn_{1.6}O_4$, but the crystalline sample revealed a mixed phase of *o*-$LiMnO_2$ and $LiMn_2O_4$ after heating at 400°C in air. The Li^+/H^+ exchange in the $Li_{1.6}Mn_{1.6}O_4$ sample progressed topotactically, while maintaining the crystal structure and morphology of the precursor. But heat-treated crystalline *o*-$LiMnO_2$ showed a disproportionation reaction with dissolution of Mn^{2+} ions.

Keywords: Solid-phase reaction; Orthorhombic lithium manganese oxide; Morphology

1. Introduction

The interesting structural and physical properties of various manganese oxide compounds have prompted a variety of applications such as adsorbents, primary precursors for pillared materials, catalysts and rechargeable batteries [1–9]. There have been numerous studies made since Gummow et al. [10] proposed the Li–Mn–O ternary phase diagram including for example, the effect of the starting materials, synthesis temperature, Li/Mn ratio, manganese oxidation state, electrochemical properties, phase transition, local structure, etc. [11–13]. Recently, Paulsen and Dahn [14] also studied the phase diagram of Li–Mn–O spinel only in air at different temperatures. Besides the solid-state reaction method at high temperature, low-temperature methods such as hydrothermal reaction, sol–gel process, intercalation, ion exchange, etc. are also used for synthesizing various manganese oxide compounds. Among these, hydrothermal synthesis at low temperature is a powerful method for synthesizing novel compounds.

Although $LiMn_2O_4$ is the most widely studied in the Li–Mn–O phase diagram [10], increasing attention is also being paid to $LiMnO_2$ samples with different crystallographic forms. $LiMnO_2$ exists in three forms: orthorhombic (*o*-$LiMnO_2$, space group *Pmnm*), monoclinic (*m*-$LiMnO_2$, space group $C2/m$) and lithiated spinel with tetragonal structure (*t*-$Li_2Mn_2O_4$, space group $I4_1/amd$). The *o*-$LiMnO_2$ samples in the literature have been prepared by hydrothermal [15,16], reflux [17], microwave irradiation [18], and solid-state reaction [19] methods with different crystallite sizes and different morphologies depending on the starting manganese precursors. Also, *o*-$LiMnO_2$ samples with varying degrees of crystallographic disorder have been prepared [20–22]. The *m*-$LiMnO_2$ was obtained either by an ion exchange reaction from α-type $NaMnO_2$ synthesized in air [23–25] or by direct hydrothermal treatment of

*Corresponding author. Fax: +81-87-869-3551.
E-mail address: chitrakar-ramesh@aist.go.jp (R. Chitrakar).
[1] Also for correspondence.

0022-4596/02/$ - see front matter
PII: S0022-4596(02)00018-X

Mn_2O_3 with a mixed solution of KOH and LiOH at 220°C [26]. The *t*-$Li_2Mn_2O_4$ was prepared by refluxing the solid $LiMn_2O_4$ with an excess of LiI dissolved in acetonitrile [27]. These $LiMnO_2$ samples have all been studied in detail for their electrochemical properties.

We previously studied the lithium extraction/insertion reaction in $L_{1.6}Mn_{1.6}O_4$ obtained from thermal decomposition of low crystalline *o*-$LiMnO_2$, which was synthesized by the hydrothermal reaction method in aqueous phase [16]. Furthermore, we also synthesized *o*-$LiMnO_2$ by microwave-assisted hydrothermal method in the same phase [18]. These synthetic methods required a large excess of $LiOH \cdot H_2O$ (Li/Mn > 7 in mole ratio). A pH-titration study showed that the proton-type sample has a lithium ion-sieve property and a high lithium uptake from seawater [17].

In the present study, we tried to obtain *o*-$LiMnO_2$ under a steam atmosphere at 120°C by directly reacting Mn-sources with $LiOH \cdot H_2O$ (Li/Mn = 1) in solid phase. The *o*-$LiMnO_2$ was also synthesized by a solid-state reaction at 700°C in nitrogen for a comparative study.

2. Experimental

2.1. Synthesis of o-$LiMnO_2$ samples

Low crystalline *o*-$LiMnO_2$ was prepared by mixing either 10.0 g of γ-MnOOH (Toyo Soda Co., Japan) or 9.0 g Mn_2O_3 (obtained by calcination of chemical grade $MnCO_3$ at 800°C for 4 h in air) with 5.0 g of $LiOH \cdot H_2O$ (Li/Mn = 1 : 1.05 in atomic ratio) in Teflon-lined stainless-steel vessels (50 cm^3) and autoclaved at 120°C for 1 day. After cooling to room temperature, the solid was dried at 60°C overnight. The obtained product (*o*-$LiMnO_2$) was then heated at 400°C for 4 h in air to obtain $Li_{1.6}Mn_{1.6}O_4$. The acid treatment of $Li_{1.6}Mn_{1.6}O_4$ was carried out batch-wise by stirring 1 g of the solid with 1 dm^3 of 0.5 mol dm^{-3} HCl solution for 2 days. The acid-treated samples were filtered and washed with deionized water and air-dried. The samples were designated as $LiMnO_2$-1, $Li_{1.6}Mn_{1.6}O_4$-1 and $H_{1.6}Mn_{1.6}O_4$-1 (all derived from γ-MnOOH), and $LiMnO_2$-2, $Li_{1.6}Mn_{1.6}O_4$-2 and $H_{1.6}Mn_{1.6}O_4$-2 (all derived from Mn_2O_3).

Crystalline *o*-$LiMnO_2$ was synthesized as follows: a known amount of $Mn(CH_3COO)_2 \cdot 4H_2O$ was dissolved in methanol and the solution was evaporated to dryness. The dried powder was heated at 450°C for 4 h in air to obtain Mn_2O_3. Mn_2O_3 powder was mixed with a slight excess of $LiOH \cdot H_2O$ (added Li/Mn = 1.5 in atomic ratio), ground, calcined at 450°C for 2 h in nitrogen, and then the temperature was increased to 700°C and maintained for a further 3 h in nitrogen. After cooling to room temperature in the nitrogen atmosphere, the solid was washed with distilled water to remove excess lithium and dried at 60°C overnight. The sample was designated as $LiMnO_2$-3. One part of this sample was then heated at 400°C and another sample at 600°C for 4 h in air and the heated samples were designated as $LiMnO_2$-3-400 and $LiMnO_2$-3-600, respectively.

2.2. Characterization

The X-ray diffraction (XRD) patterns were taken on a Rigaku-type RINT 1200 X-ray diffractometer with a graphite monochromator with Cu$K\alpha$ radiation (λ = 1.5406). DTA-TG curves of materials were obtained on a MAC science thermal analyzer (System 001, 200 TG-DTA) at a heating rate of 10°C/min in air. Fourier transform infrared (FT-IR) spectra were recorded on a Perkin-Elmer System 2000 infrared spectrophotometer, using a KBr technique; 300 hundred scans were averaged with a nominal resolution of 4 cm^{-1}. The SEM photographs of various materials were taken on a Hitachi-type S-2460 N scanning electron microscope.

Chemical analysis of lithium and manganese was carried out by using atomic absorption spectroscopy. The mean oxidation state of manganese (Z_{Mn}) was determined by reducing the solid to Mn^{2+} ions with sodium oxalate solution in sulfuric acid solution and back titrating the excess sodium oxalate solution with standard potassium permanganate solution as described in the literature [28].

2.3. Uptake of lithium from LiCl-enriched seawater

The uptake of Li^+ from lithium-enriched seawater was determined by stirring 100 mg of acid-treated solids in 1 dm^3 of seawater (Li^+ concentration: 5 mg dm^{-3}) for 1 week at room temperature. After attainment of equilibrium, the Li^+ ion content in the supernatant solution was determined.

3. Results and discussion

3.1. Characterization of low crystalline o-$LiMnO_2$

We carried out a direct solid-phase reaction between Mn-precursor and $LiOH \cdot H_2O$ at 120°C in a closed system. The lithium insertion reaction in γ-MnOOH was monitored by analyzing the Li/Mn ratio in the product at different intervals (Fig. 1). The reaction proceeded only after 4 h and it was complete at 24 h. All the other autoclave reactions were therefore carried out for 24 h. In the γ-MnOOH–$LiOH \cdot H_2O$ system at 120°C and under 2 bars of pressure, the vapor arising from $LiOH \cdot H_2O$ may strengthen the reactivity of LiOH at the surface of MnOOH particles, which may enable the slow diffusion of Li^+ ions into MnOOH particles. The

Li^+/H^+ exchange reaction may progress slowly to form $LiMnO_2$. In the Mn_2O_3–$LiOH \cdot H_2O$ system also, Mn_2O_3 particles change to $LiMnO_2$. The reaction was assumed to be a lithiation process since there are no lattice protons in Mn_2O_3. The analyzed Li/Mn molar ratios and Z_{Mn} values for the samples are given in Table 1. Although the Li/Mn starting ratio of 1 was effectively retained in the samples, the mean oxidation state of manganese was found to be slightly high. The calculated compositions closely approached the theoretical formula $LiMnO_2$.

An attempt to prepare $LiMnO_2$ samples by reacting γ-MnOOH or Mn_2O_3 with $LiOH \cdot H_2O$ under an open atmosphere at 120°C was unsuccessful; the reaction did not progress at all. This indicates that the water vapor plays an important role in the formation of *o*-$LiMnO_2$.

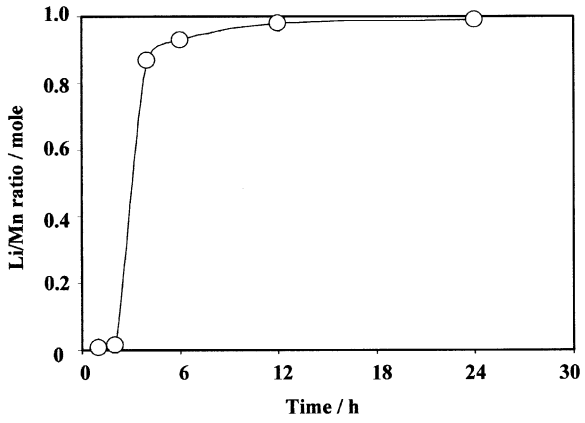

Fig. 1. Li/Mn ratio in *o*-$LiMnO_2$ at different intervals. γ-MnOOH = 10.0 g, $LiOH \cdot H_2O$ = 5.0 g, autoclave vessel = 50 cm^3, Temp. = 120°C.

The XRD patterns of $LiMnO_2$-1 and $LiMnO_2$-2 exhibited broad and ill-defined peaks as compared to the starting Mn-sources (Fig. 2). All the diffraction peaks could be indexed according to the space group *Pmnm* of the orthorhombic structure. The lattice parameters of the present samples were nearly the same as the sample reported in the literature (Table 1). The presence of peak broadening in both samples suggested the existence of structural disorders between Li and Mn sites. According to Croguennec et al. [21] the full-width at half-maximum (FWHM) of the (011) peak in the XRD patterns could be correlated with the density of the monoclinic stacking faults occurring in *o*-$LiMnO_2$. This approach was further applied to different *o*-$LiMnO_2$ samples by other researchers [29,30]. The FWHM of (011) peak at $2\theta = 24.8^\circ$ of 0.85° in the present samples (Fig. 2) corresponded to 4% stacking faults according to their analysis [21], suggesting that the present samples have a disordered orthorhombic structure. We applied a similar approach in a previous study [18]. The FT-IR spectrum of $LiMnO_2$-1 and $LiMnO_2$-2 are shown in Fig. 3; these two samples showed absorption bands at 3450 cm^{-1}, which could be assigned to the stretching vibration due to adsorbed water from atmosphere. γ-MnOOH showed absorption band at 2677 cm^{-1}, probably due to O–H stretching vibration; this band disappeared after the reaction with $LiOH \cdot H_2O$. This suggests that the low-temperature *o*-$LiMnO_2$ does not contain H in the bulk sample and the reaction between γ-MnOOH and LiOH progresses by ion-exchange-type reaction. Most of the bands in the lower

Table 1
Chemical compositions and lattice parameters of different materials

Sample	Li/Mn	H_2O/Mn	Z_{Mn}	Chemical composition	Present work	Literature cited
$LiMnO_2$-1	1.00	—	3.16	$LiMnO_{2.10}$	$a = 2.81$ Å $b = 5.75$ Å $c = 4.57$ Å (Orthorhombic, *Pmnm*)	$a = 2.80(5)$ Å $b = 5.75(7)$ Å $c = 4.57(2)$ Å (Ref. [19])
$LiMnO_2$-2	1.01	—	3.22	$LiMnO_{2.11}$	$a = 2.81$ Å $b = 5.75$ Å $c = 4.56$ Å	”
$LiMnO_2$-3	1.01	—	3.0	$LiMnO_2$	$a = 2.81$ Å $b = 5.75$ Å $c = 4.57$ Å	”
$Li_{1.6}Mn_{1.6}O_4$-1	1.01	—	3.95	$Li_{1.64}Mn_{1.61}O_4$	$a = 8.14$ Å (Cubic, *Fd3m*)	$a = 8.14$ Å (Ref. [16])
$Li_{1.6}Mn_{1.6}O_4$-2	1.00	—	3.95	$Li_{1.63}Mn_{1.61}O_4$	$a = 8.13$ Å	”
$LiMnO_2$-3-400	1.01	—	Not determined	$LiMnO_2$ phase + traces $LiMn_2O_4$	—	—
$H_{1.6}Mn_{1.6}O_4$-1	0.07	0.51	3.99	$H_{1.62}Li_{0.11}Mn_{1.57}O_4$	$a = 8.05$ Å (Cubic, *Fd3m*)	$a = 8.05$Å (Ref. [16])
$H_{1.6}Mn_{1.6}O_4$-2	0.03	0.52	3.98	$H_{1.65}Li_{0.05}Mn_{1.58}O_4$	$a = 8.05$ Å	”
$LiMnO_2$-3-400(H)	0.21	0.24	Not determined	—	—	—

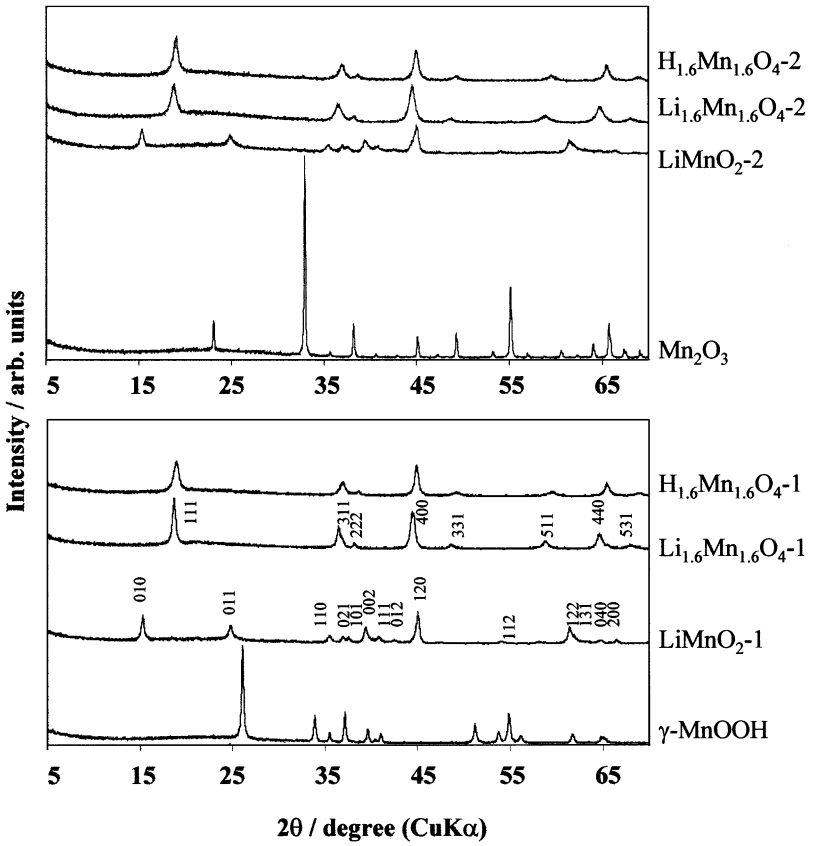

Fig. 2. XRD patterns of Mn precursors, *o*-$LiMnO_2$ and $H_{1.6}Mn_{1.6}O_4$ samples.

wave number region (below 800 cm^{-1}) were attributed to the vibrations of MnO_6 octahedra. Fig. 4 shows the SEM photographs of $LiMnO_2$-1 and $LiMnO_2$-2 with needle-shaped and spherical morphologies identical to their Mn precursors. The SEM results indicated that the morphology was unaffected by ion exchange or lithiation process.

3.2. Characterization of crystalline o-$LiMnO_2$

The XRD patterns of samples prepared by solid-state reaction at high temperature are shown in Fig. 5. $LiMnO_2$-3 was obtained as a crystalline material and all the peaks of the XRD pattern could be indexed to orthorhombic structure with nearly the same lattice parameters as the low crystalline samples (Table 1). The FWHM of (011) peak in Fig. 5 at $2\theta = 24.8^\circ$ was $<0.15^\circ$, which suggested that the sample has a well-ordered orthorhombic structure with fewer stacking faults (1%), according to the analysis [21]. The *o*-$LiMnO_2$ samples with stacking faults less than 1% have also been prepared by other researchers, who concluded that the samples had a well-ordered orthorhombic structure [29,30]. The analyzed Li/Mn molar ratio was 1 with a Z_{Mn} value of 3 (Table 1). The FT-IR of $LiMnO_2$-3 showed bands at 598 and 484 cm^{-1}, which could be assigned to Mn–O stretching vibrations (Fig. 3). The SEM images of the $LiMnO_2$-3 showed octahedron particles 2–3 μm in size, the morphology being different from the starting Mn-source (Fig. 4). From SEM observations, it was clear that the surface of the sample was smooth and homogeneous and crystal size was also larger as compared to $LiMnO_2$-1 and $LiMnO_2$-2.

3.3. Heat-treated samples

$LiMnO_2$-1 and $LiMnO_2$-2 were known to have stacking faults and thus possessed structural defects. The heat treatment of these samples at 400°C in air brought about the formation of $Li_{1.6}Mn_{1.6}O_4$ due to the oxidation of manganese from trivalent to tetravalent. Due to the structural defects of $LiMnO_2$, the particles were likely to have been sufficiently in contact with oxygen during the heat treatment in air. The thermal decomposition behaviors of these samples are shown in Fig. 6. The DTA-TG curve of $LiMnO_2$-1 showed an exothermic peak at 356°C with weight gain, and the weight loss and gain could be observed around 400°C and 500°C, respectively. The thermal decomposition temperature of $LiMnO_2$-2 was 335°C with weight gain after which there was a sudden weight decrease with rise

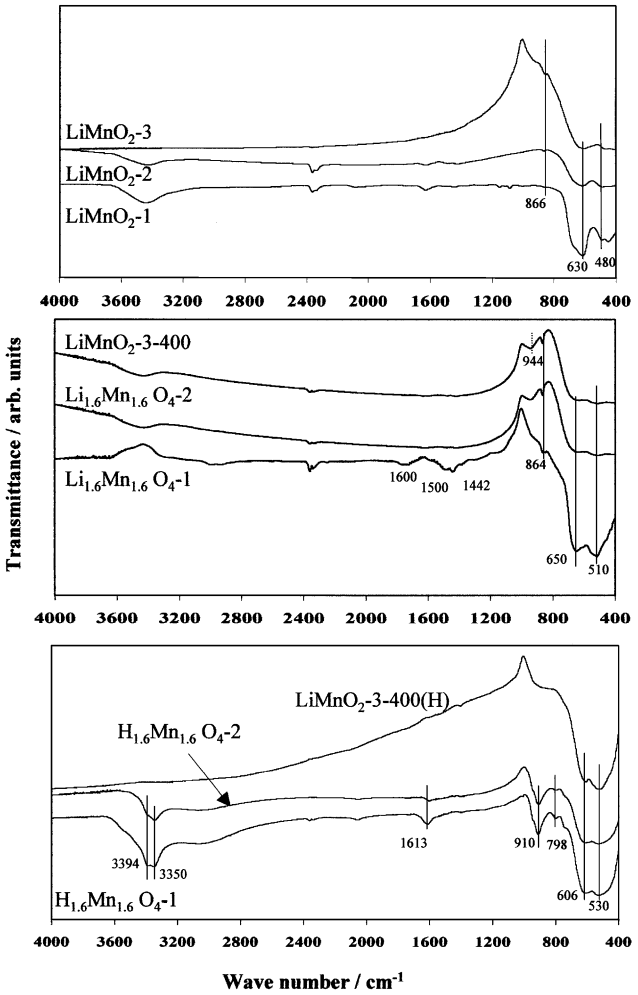

Fig. 3. FT-IR spectra of $LiMnO_2$ and its heat- and acid-treated samples.

in temperature till 420°C. The decomposition temperatures of *o*-$LiMnO_2$ samples prepared by the hydrothermal method [16] and microwave irradiation method [18] in aqueous phase were 380°C and 320°C, respectively. The difference in thermal decomposition of *o*-$LiMnO_2$ samples prepared by different methods might be due to differences in crystallinity. It was found that the peak intensities of the XRD patterns of the sample obtained by the hydrothermal method in aqueous phase were slightly higher than those of samples obtained by other methods. The sample with higher crystallinity would have a higher decomposition temperature. When the $LiMnO_2$ samples were heated at 400°C for 4 h in air, the weight gain was about 6%, which corresponded to the conversion from $LiMnO_{2.1}$ to $LiMnO_{2.5}$ ($Li_{1.6}Mn_{1.6}O_4$). The analyzed Li/Mn molar ratios were almost 1 with manganese mean oxidation of 3.96 (Table 1).

The XRD patterns of heat-treated samples are shown in Fig. 2 and all the peaks could be indexed according to the space group *Fd*3*m* of cubic structure with lattice parameter $a = 8.14$ Å (Table 1). Pure spinel-type lithium manganese oxides with Li/Mn molar ratios from 0.5 to 0.8 were synthesized by directly heating a mixture of $MnCO_3$ and Li_2CO_3 at 400°C in air, and a mixture of spinel-type and monoclinic-type $LiMnO_3$ was formed with $Li/Mn > 1$ at 400°C in air [31]. In the present study, we also tried to prepare $Li_{1.6}Mn_{1.6}O_4$ by heating a mixture of $MnCO_3$ and Li_2CO_3 with $Li/Mn = 1$ at 400°C in air, but the resultant heat-treated sample was a mixture of spinel type ($Li_{1.33}Mn_{1.67}O_4$) and Li_2MnO_3. This result suggests that direct synthesis of $Li_{1.6}Mn_{1.6}O_4$ by solid-state reaction is not possible.

The *o*-$LiMnO_2$ can be classified as a rock salt structure in which the Mn and Li ions form independent sheets of MnO_6 and LiO_6 octahedra that are arranged in corrugated (zig-zag) layers. Due to the manganese (d^4) electronic configuration, the oxygen octahera around Mn^{3+} in *o*-$LiMnO_2$ is quite asymmetric (Jahn Teller Deformation). The oxidation of *o*-$LiMnO_2$ leading to a more symmetrical manganese Mn^{4+} (d^{3+}) is rather likely to induce some structural rearrangement or even straightforward structural transition towards a higher symmetry. Transformation of the *o*-$LiMnO_2$ to the spinel-type lithium manganese oxide has been explained by different researchers [32–34]. The displacement of Mn atoms into neighboring vacant octahedral sites causes the displacement of the other Mn atoms. This transformation is caused by a displacement of 50% of the Mn atoms to generate the 3:1 ratio of Mn atoms in alternate layers between layers of cubic closed packed oxygen planes, which is required by the ideal $Li[Mn_2]O_4$. This normal spinel structure possesses the crystallographic space group *Fd*3*m*, where Li ions occupy 8*a* tetrahedral sites and Mn ions occupy 16*d* octahedral sites in a cubic closed packed array of oxygen ions. We carried out Rietveld and TEM analyses for Li and Mn atoms distribution in $Li_{1.6}Mn_{1.6}O_4$. The $Li_{1.6}Mn_{1.6}O_4$ was found to be a lithium-rich cubic spinel where some of the Mn atoms were displaced by the Li atoms. The formula could be written as $(Li)_{8a}[Li_{0.5}Mn_{1.5}]_{16d}O_{3.75}$ with excess Li and Mn atoms in 16*d* sites of spinel notation having oxygen deficiency. A paper on structural refinement of $Li_{1.6}Mn_{1.6}O_4$ using Rietveld and TEM analyses is in progress for submission.

The FT-IR spectrum of $Li_{1.6}Mn_{1.6}O_4$-1 and $Li_{1.6}Mn_{1.6}O_4$-2 is shown in Fig. 3. Small bands at 1500 and 1442 cm^{-1} were attributed to carbonate stretching vibration and 944 and 844 cm^{-1} to carbonate lattice vibration. The bands (650 and 510 cm^{-1}) in the regions below 800 cm^{-1} were shifted to a slightly higher wave number as compared to $LiMnO_2$ samples.

The DTA-TG curve of $LiMnO_2$-3 showed a small exothermic peak at 608°C with weight gain from 400°C till a constant weight was reached at 800°C (Fig. 6). This decomposition temperature was much higher than that

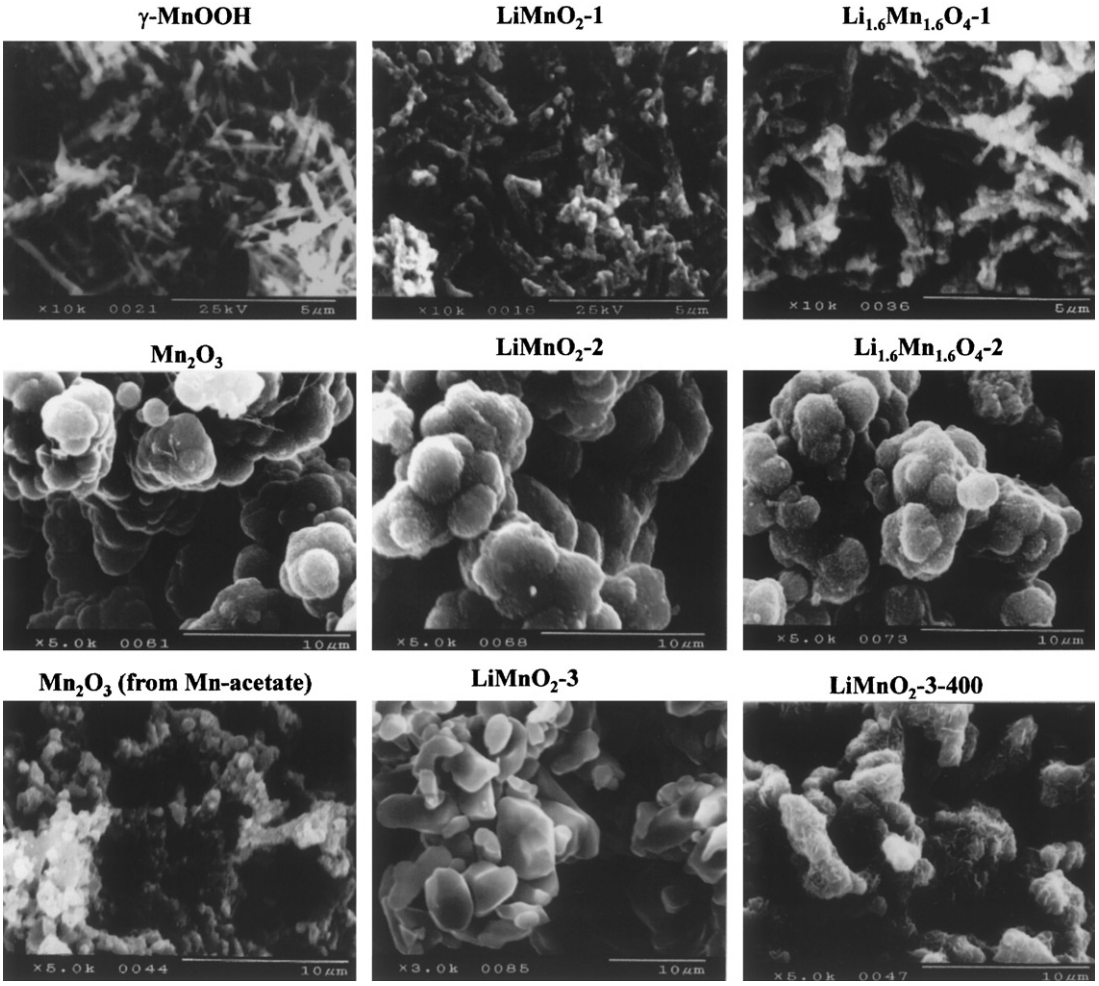

Fig. 4. SEM photographs of different samples.

of $LiMnO_2$-1 or $LiMnO_2$-2. The XRD pattern of $LiMnO_2$-3 heated at 400°C in air ($LiMnO_2$-3-400) still showed major peaks corresponding to *o*-$LiMnO_2$ with traces of $LiMn_2O_4$ (Fig. 5). The XRD patterns of $LiMnO_2$-3 heated at 600°C in air ($LiMnO_2$-3-600) showed peaks of monoclinic Li_2MnO_3 and spinel $LiMn_2O_4$ (Fig. 5). Crystalline *o*-$LiMnO_2$ is known to decompose to a mixture of Li_2MnO_3 with monoclinic phase and $LiMn_2O_4$ with spinel phase after heating at 500°C in air [33]. Attempts to prepare a single phase of cubic $Li_{1.6}Mn_{1.6}O_4$ by the heat treatment of $LiMnO_2$-3 were unsuccessful in the present study.

The FT-IR spectra of $LiMnO_2$-3-400 are shown in Fig. 3. A small band around 3400 cm^{-1} could be assigned to the stretching vibration of adsorbed water from the atmosphere. The two bands at 944 and 865 cm^{-1} due to carbonate were also observed. The bands at 650 and 510 cm^{-1} were due to Mn–O stretching vibrations; these two bands were shifted to a higher wave number as compared to $LiMnO_2$-3. The SEM image recorded for $LiMnO_2$-3-400 sample is quite different from $LiMnO_2$-3 (Fig. 4), because thermal decomposition of $LiMnO_2$-3 at 400°C in air leads to the formation of a mixture of $LiMnO_2$ and $LiMn_2O_4$. A mixture of the two oxides could be clearly seen in the $LiMnO_2$-3-400 sample showing large crystals of $LiMnO_2$ with small attached fibrous particles of $LiMn_2O_4$.

3.4. Acid-treated materials

Chemical analysis showed that 93% and 96% of the original lithium contents in $Li_{1.6}Mn_{1.6}O_4$-1 and $Li_{1.6}Mn_{1.6}O_4$-2, respectively, were extracted with a 0.5 mol dm^{-3} HCl solution, with little dissolution of Mn^{2+} ions (2%). These two samples with tetravalent manganese formed stable protonated sites according to the topotactic Li^+/H^+ exchange reaction without a disproportionation reaction and such acid-treated samples should act as lithium-selective adsorbents. The mean oxidation states of manganese in $H_{1.6}Mn_{1.6}O_4$-1 and $H_{1.6}Mn_{1.6}O_4$-2 were nearly equal to 4 (Table 1). The lattice proton content was evaluated by the weight loss between 100°C and 400°C in the TG curve, assuming the

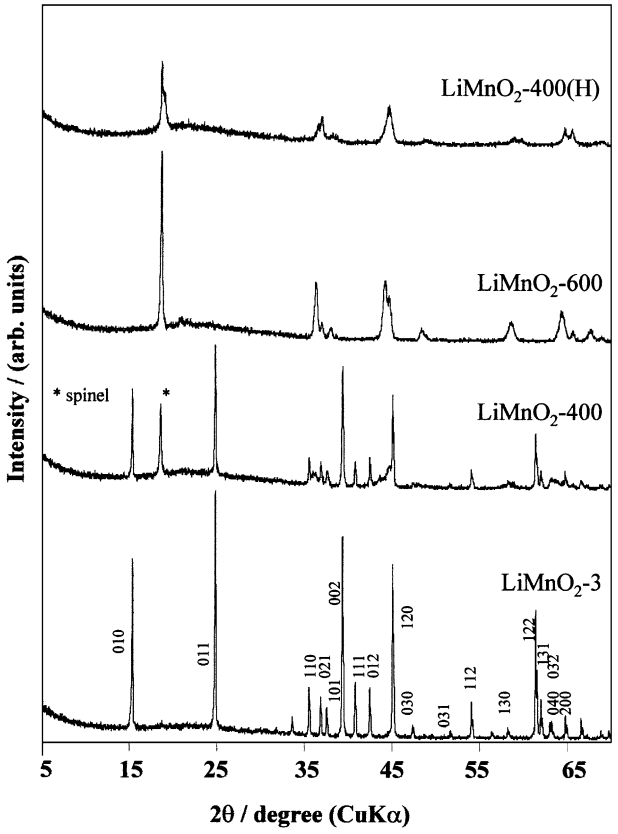

Fig. 5. XRD patterns of crystalline o-$LiMnO_2$ and its heat- and acid-treated samples.

product to be β-MnO_2 at 400°C. The H_2O contents were nearly equal to the theoretical proton content calculated based on the Li^+/H^+ exchange reaction, suggesting that the H_2O contents corresponded to the number of lattice hydroxyl groups formed by the exchange reaction. Calculation of the chemical composition of the acid-treated samples showed the presence of small amount of un-reacted lithium as an impurity (Table 1).

The XRD patterns of $H_{1.6}Mn_{1.6}O_4$-1 and $H_{1.6}Mn_{1.6}O_4$-2 showed the preservation of the cubic structure with a slight decrease in the lattice constant of $a = 8.05$ Å, while the relative intensities of the peaks were almost the same as the precursor $Li_{1.6}Mn_{1.6}O_4$ (Fig. 2).

The DTA-TG curves of $H_{1.6}Mn_{1.6}O_4$-1 show two small endothermic peaks at 149°C and 195°C with weight loss, while $H_{1.6}Mn_{1.6}O_4$-2 shows only one small endothermic peak at 192°C with weight loss (Fig. 6). The temperature (195°C), where the endothermic peaks were observed, was higher than the usual evaporation temperature of water (100°C); so these samples contained crystal water or lattice hydroxyl groups in a more ordered state, which was further confirmed from FT-IR results. The complete evaporation of these lattice hydroxyl groups was followed by the transformation from the cubic structure to β-MnO_2. The large endothermic peaks at 537°C and 531°C for both samples with weight loss were due to the transformation from β-MnO_2 to the more stable α-Mn_2O_3 phase accompanied by loss of oxygen.

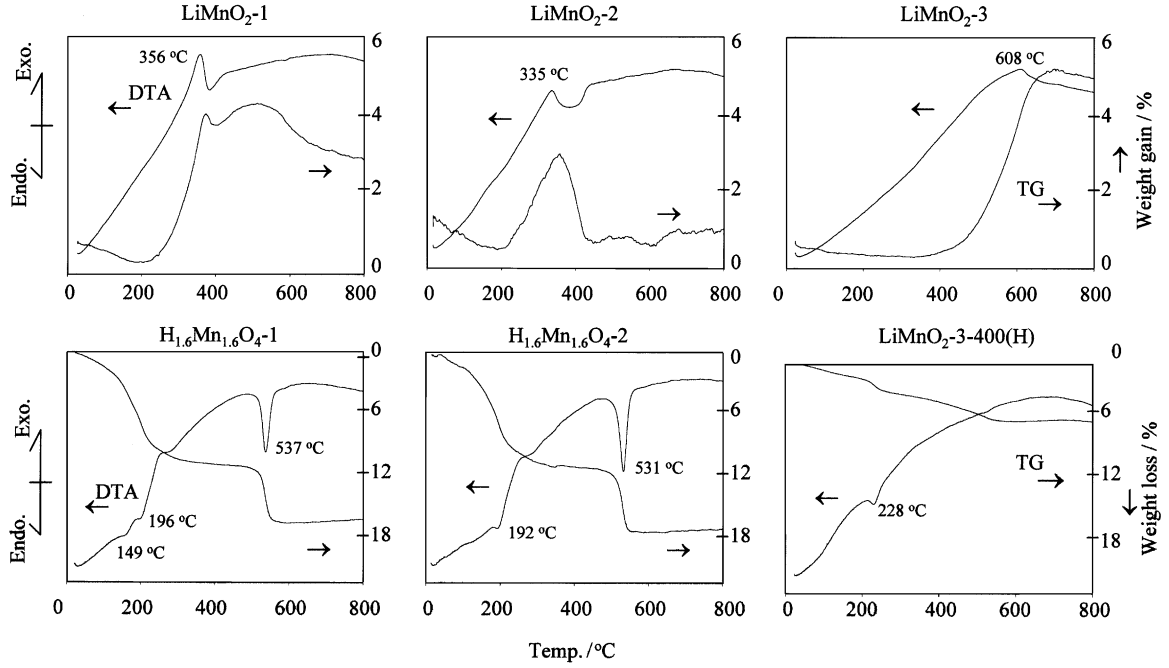

Fig. 6. DTA-TG curves of different samples.

The FT-IR of $H_{1.6}Mn_{1.6}O_4$-1 and $H_{1.6}Mn_{1.6}O_4$-2 showed two distinct bands resolved at 3350 and 3394 cm^{-1}, which were due to the stretching vibration of hydroxyl groups (Fig. 3). These two bands were usually associated with the band at 910 cm^{-1}, which was due to lattice coupling vibration and suggested the presence of hydroxyl groups in a more ordered state. Similar results were also observed on crystalline sample obtained by acid treatment of spinel-type lithium manganese oxide [35]. The band at 1613 cm^{-1} could be ascribed to the bending vibrations of the lattice –OH groups.

The acid treatment of $LiMnO_2$-3-400 led to a disproportionation-type reaction with Li^+ extractability of 78 wt% and Mn^{2+} ion dissolution of 20 wt%. Chemical analysis showed that the Li/Mn mole ratio in aqueous phase after acid treatment was 2.1, which was close to the theoretical value (dissolved Li/dissolved Mn = 2) based on the disproportionation reaction of $LiMnO_2$ as follows:

$$LiMn(III)O_2 + 4xH^+ \rightarrow Li_{3-2x}Mn(III)_{3-2x}Mn(IV)_xO_{6-2x} + xMn^{2+} + 2xLi^+ + 2xH_2O.$$

On the other hand, the Li^+ ion extractability from the $LiMnO_2$-3-600 sample was only 55 wt% with 7 wt% dissolution of Mn^{2+} ions; the low Li^+ extractability was due to the presence of Li_2MnO_3 phase, as it was confirmed from the XRD patterns (Fig. 5). It is well known that the extraction of Li^+ from Li_2MnO_3 is very difficult by a similar acid treatment [36].

The DTA-TG curve of the acid-treated sample $LiMnO_2$-3-400(H) is shown in Fig. 6. There was a small endothermic peak at 228°C with weight loss. The weight loss continued until 500°C and no endothermic peak was observed around 530°C. The evaluated lattice proton content in $LiMnO_2$-3-400(H) sample was nearly 1/4 due the disproportionation reaction as compared to $H_{1.6}Mn_{1.6}O_4$ samples.

3.5. Li^+ uptake from LiCl-enriched seawater

The Li^+ uptake from LiCl-enriched seawater was investigated with acid-treated samples. The Li^+ uptakes by $H_{1.6}Mn_{1.6}O_4$-1 and $H_{1.6}Mn_{1.6}O_4$-2 were 4.75 mmol/g (33 mg/g), while the uptake was less than 0.10 mmol/g by $LiMnO_2$-3-400(H). These results confirmed that adsorbents derived from low crystalline *o*-$LiMnO_2$ were highly selective for Li^+ ions only, and were non-selective for alkali and alkaline earth metal ions in seawater. Chemical analysis revealed that the adsorbent derived from the highly crystalline *o*-$LiMnO_2$ sample contained 20% of the original Li^+ ions after acid treatment, and the content of lattice protons was markedly smaller than the other $H_{1.6}Mn_{1.6}O_4$ samples, resulting in the adsorbent showing a negligible amount of Li^+ ion uptake in seawater.

4. Conclusion

Low crystalline *o*-$LiMnO_2$ samples with structural defects were successfully prepared by a solid-phase reaction under steam atmosphere at 120°C. These samples after heat treatment at 400°C in air were easily converted to cubic $Li_{1.6}Mn_{1.6}O_4$. The acid-treated samples ($H_{1.6}Mn_{1.6}O_4$) showed lithium ion-sieve properties. Crystalline *o*-$LiMnO_2$ consisted of well-ordered particles and was converted to a mixture of $LiMnO_2$ and $LiMn_2O_4$ at 400°C in air and finally to a mixture of Li_2MnO_3 and $LiMn_2O_4$ at 600°C in air and their acid-treated samples did not have lithium ion-sieve properties. Synthetic conditions should be directed towards creating the structural defects in order to obtain lithium-ion-selective adsorbents. The present technique can be presumably used to prepare other manganese oxides with different crystal structures.

References

[1] M.M. Thackeray, Prog. Solid State Chem. 25 (1997) 1.
[2] X.M. Shen, A. Clearfield, J. Solid State Chem. 64 (1986) 270.
[3] K. Ooi, Y. Miyai, J. Sakakihara, Langmuir 7 (1991) 1167.
[4] S.L. Brock, N. Duan, Z.R. Tian, O. Giraldo, H. Zhou, S.L. Suib, Chem. Mater. 10 (1998) 2619.
[5] R. Chen, P. Zavalij, M.S. Whittingham, Chem. Mater. 8 (1996) 1275.
[6] S. Ching, P.F. Driscoll, K.S. Kieltyka, M.R. Marvel, S.L. Suib, Chem. Comm. (2001) 2486.
[7] Z. Liu, K. Ooi, H. Kanoh, W. Tang, T. Tomida, Langmuir 16 (2000) 4156.
[8] Q. Gao, O. Giraldo, W. Tong, S.L. Suib, Chem. Mater. 13 (2001) 778.
[9] J. Kim, A. Manthiram, Nature 390 (1997) 265.
[10] R.J. Gummow, A. De Kock, M.M. Thackeray, Solid State Ionics 69 (1994) 59.
[11] C. Masquelier, M. Tabuchi, K. Ado, R. Kanno, Y. Kobayashi, Y. Maki, O. Nakamura, J.B. Goodenough, J. Solid State Chem. 123 (1996) 255.
[12] Y.J. Lee, F. Wang, C.P. Grey, J. Am. Chem. Soc. 120 (1998) 12601.
[13] B. Ammundsen, D.J. Jones, J. Rozière, G.R. Burns, Chem Mater. 8 (1996) 2799.
[14] J.M. Paulsen, J.R. Dahn, Chem Mater. 11 (1999) 3065.
[15] M. Tabuchi, K. Ado, C. Masquelier, I. Matsubara, H. Sakaebe, H. Kageyama, H. Kobayashi, R. Kanno, O. Nakamura, Solid State Ionics 89 (1996) 53.
[16] R. Chitrakar, H. Kanoh, Y. Miyai, K. Ooi, Chem. Mater. 12 (2000) 3151.
[17] R. Chitrakar, H. Kanoh, Y. Miyai, K. Ooi, Ind. Eng. Chem. Res. 40 (2001) 2054.
[18] R. Chitrakar, H. Kanoh, Y. Miyai, K. Ooi, J. Solid State Chem. 163 (2002) 1.
[19] J.N. Reimers, E.W. Fuller, E. Rossen, J.R. Dahn, J. Electrochem. Soc. 140 (1993) 3396.

[20] L. Croguennec, P. Deniard, R. Brec, P. Biensan, M. Broussely, Solid State Ionics 89 (1996) 127.
[21] L. Croguennec, P. Deniard, R. Brec, A. Lecerf, J. Mater. Chem. 7 (1997) 511.
[22] L. Croguennec, P. Deniard, R. Brec, J. Electrochem. Soc. 144 (1997) 3323.
[23] A.R. Armstrong, P.G. Bruce, Nature 381 (1996) 499.
[24] G. Vitins, K. West, J. Electrochem. Soc. 144 (1997) 2587.
[25] R. Chitrakar, H. Kanoh, Y.-S. Kim, Y. Miyai, K. Ooi, J. Solid State Chem. 160 (2001) 69.
[26] M. Tabuchi, K. Ado, H. Kobayashi, H. Kageyama, J. Electrochem. Soc. 145 (1998) L49.
[27] J.M. Tarascon, D. Guyomard, J. Electrochem. Soc. 138 (1991) 2864.
[28] Japan Industrial Standard (JIS), M8233, 1969.
[29] Y.-I. Jang, B. Huang, H. Wang, D.R. Sadoway, Y.-M. Chiang, J. Electrochem. Soc. 146 (1999) 3217.
[30] Y.-M. Chiang, D.R. Sadoway, Y.-I. Jang, B. Huang, H. Wang, Electrochem. Solid-State Lett. 2 (1999) 107.
[31] Q. Feng, Y. Miyai, H. Kanoh, K. Ooi, Langmuir 8 (1992) 1861.
[32] R.J. Gummow, D.C. Liles, M.M. Thakeray, Mat. Res. Bull. 28 (1993) 1249.
[33] W. Tang, H. Kanoh, K. Ooi, J. Solid State Chem. 142 (1999) 19.
[34] Y.-M. Chiang, H. Wang, Y.-I. Jang, B. Huang, Chem. Mater. 13 (2001) 53.
[35] B. Ammundsen, P.B. Aitchison, G.R. Burns, D.J. Jones, J. Rozière, Solid State Ionics 97 (1997) 269.
[36] W. Tang, H. Kanoh, X. Yang, K. Ooi, Chem. Mater. 12 (2000) 3271.